frontiers in Mechanical Engineering

ORIGINAL RESEARCH
published: 05 October 2020
doi: 10.3389/fmech.2020.566440

Friction Influenced by Vibrations: A Refined Contact-Mechanics View on Lateral and Rotational Oscillations

*Roman Pohrt**

Department of System Dynamics and Friction Physics, Institute of Applied Mechanics, Technische Universität Berlin, Berlin, Germany

It is known that superposed movements can lower the friction felt at the macroscale. This is well documented for in-plane and normal translatory oscillations. Contact mechanics are a suitable approach to model this effect but so far have not gone beyond single-slider dynamics. In this study, we make use of 3D Boundary Elements Simulations to study the macroscopic friction reduction. This approach allows us to take into account also partial sliding of the contact zone. We first revisit the case of transversal in-plane translatory oscillations. Here, we argue that the behavior at small velocities can best be described when partial slip is indeed taken into account. Next, we investigate the frictional response of a Hertzian indenter when the lateral movement is superposed with a rotational bore movement. An analytical approximation is given for the steady state solution with constant angular velocity. The third case under investigation is an oscillating bore rotation. We present numerical results for the reduction of the macroscopic friction. In two limiting cases, an analytical prediction is given, following the lines used in the translatory case. For extremely large amplitudes, it is based on the idea that a rotational steady state is assumed at every instant. For small velocities we adapt our new approach including partial sliding. We find these predictions to be good but not perfect, slightly underestimating the reduction that rotational oscillations can provide.

Keywords: friction, vibrations, microslip, fretting, shakedown

OPEN ACCESS

Edited by:
Marco Paggi,
IMT School for Advanced Studies Lucca, Italy

Reviewed by:
Carmine Putignano,
Politecnico di Bari, Italy
Ken Nakano,
Yokohama National University, Japan

***Correspondence:**
Roman Pohrt
roman.pohrt@tu-berlin.de

Specialty section:
This article was submitted to Tribology, a section of the journal Frontiers in Mechanical Engineering

Received: *28 May 2020*
Accepted: *14 September 2020*
Published: *05 October 2020*

Citation:
Pohrt R (2020) Friction Influenced by Vibrations: A Refined Contact-Mechanics View on Lateral and Rotational Oscillations. Front. Mech. Eng. 6:566440. doi: 10.3389/fmech.2020.566440

INTRODUCTION

When frictional contacts are subjected to external oscillations, the friction felt at the macroscale is generally reduced. Since this constitutes a relatively simple way to control friction, the effect is used in countless manufacturing applications (Siegert and Ulmer, 2001a; Siegert and Ulmer, 2001b; Murakawa, 2001; Egashira and Mizutani, 2002; Ashida and Aoyama, 2007) as well as in noise control (Thomsen, 1999). On the negative side, it can lead to an error in measurements of the coefficient of friction (Kado et al., 2014).

The effect has been described experimentally in the middle of the last century (Fridman and Levesque, 1959; Pohlman and Lehfeldt, 1966; Godfrey, 1967; Lenkiewicz, 1969) but modeling was not attempted. In 2002, Storck (2002) investigated translatory in-plane oscillations experimentally and analytically. They argued that the interplay of forward friction and the superposed vibrations can be modeled using the perspective of contact mechanics with the simple Coulomb law of friction of a single slider. Kumar and Hutchings (2004) use a comparable modeling to interpret their experimental data. Tsai and Tseng (2005) employed the Dahl friction

model to estimate the reduction for in-plane oscillations and found that rigid slider models overestimate the friction reduction. Teidelt, (2012) reported an impressive series of experimental data on the reduction for oscillations in the two in-place directions as well as the out-of-plane direction and interpreted the results using a model of rigid sliders. Starcevic and Filippov also worked on this dataset. They used the Method of Dimensionality Reduction to study static friction under the influence of in-plane parallel oscillations. Their setup consisted of two coupled parabolic sliders and included micro-slip (Starcevic and Filippov, 2012). The same method was used by Teidelt et al. (2012) to study the performance of Microdrive actuators. The simultaneous acting of normal and in-plane-parallel oscillation was studied by Popov and Li (2018) using an elastic slider model. The case of in-plane oscillation transversal to the macroscopic forward motion was modeled in a recent study by Benad et al., (2019). They used a coulomb-type frictional slider attached to a linear spring. In this work, results are given as a function of normalized input quantities and explicit dependencies are given for two limiting cases, corresponding to very low forward velocities (static friction) on the one hand and very large oscillation amplitudes on the other hand. Their work can be considered the starting point of the current paper. *"Transverse Oscillations"* section of the current paper will build on their results but will introduce explicit partial slip.

The setup under investigation is the following: We focus solely on superposed in-plane motion, leaving the normal contact unchanged. Unless stated otherwise, the indenter is a sphere with radius R, approximated by a parabola shape. It is compressed elastically against a non-deformable flat counterbody. The resulting contact zone and normal stresses are of the Hertzian type and are assumed to be unaffected by tangential stresses. The elastic sphere and the rigid counterbody interact locally with a constant coefficient of friction μ, such that the effective tangential stress inside the contact zone is always less or equal to the normal stress at that point. While the indentation depth in normal direction (z) is held constant, the sphere is subjected to controlled in-plane displacements. *"Transverse Oscillations"* section will start with a constant velocity in forward (x) direction and harmonic oscillation in y-direction. In *"Continuous Rotation (Bore)"* section, the sphere will also move with constant velocity but will also rotate (bore) around its central z-axis at constant angular velocity. *"Oscillating Rotation (Bore)"* section will cover the case of oscillatory bore rotation. In all cases, the macroscopic forward friction will be decreased. The greatest reduction is generally associated with larger amplitude, frequency or velocity, respectively, of the superposed motion.

TRANSVERSE OSCILLATIONS

The case of transverse oscillations consists of a frictional indenter which is moved with constant velocity in x-direction while its position in y-direction is given by a sine-function

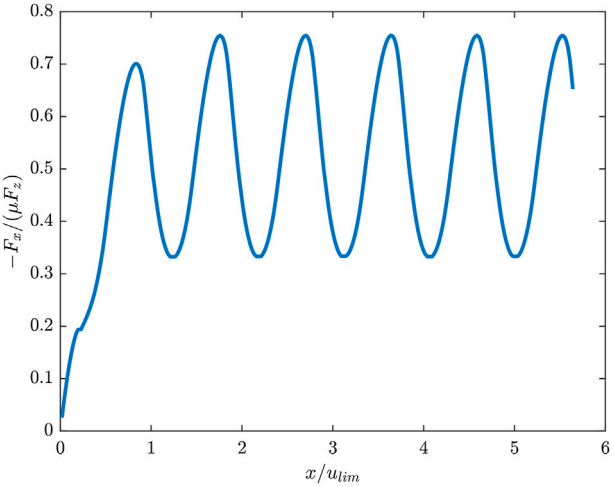

FIGURE 1 | Dependency of the normalized tangential force on the displacement when transverse oscillations are applied. Here $\tilde{v}_0 = 0.3$ and $\tilde{y}_0 = 1.6$ were chosen. The resulting effective coefficient of friction is $\tilde{\mu}_{macro} \approx 0.53$.

$$\begin{aligned} x(t) &= v_0 \cdot t \\ y(t) &= y_0 \sin(\omega_{\text{transv}} t) \end{aligned} \tag{1}$$

The simplest approach is to assume that **Eq. 1** describe not only the macroscopic motion of the indenter but also the exact motion of the *contact spot*. This approach neglects the lateral elasticity of the indenter. In contrast, the model of Benad et al. (2019) consists of a single slider but connected to the coordinates given in **Eq. 1** by a linear spring. They showed that the stiffness has a considerable influence on the system behavior, in particular for small oscillation amplitudes. We agree with this assessment. Because the system is quasistatic, it makes sense to formulate in problem in a way that eliminates the time. Similar to Benad et al. (2019), we employ a set of two dimensionless variables for such system including elasticity. The amplitude of the oscillation is described as

$$\tilde{y}_0 = \frac{y_0}{u_{\text{lim}}} \tag{2}$$

where $u_{\text{lim}} = \mu d \frac{E^*}{G^*}$ is the maximum unidirectional tangential displacement of the indenter before full sliding occurs, see (Mindlin, 1949; Popov, 2019). Here d is the indentation depth in normal direction, $E^\star$, $G^\star$ are the reduced moduli of shear and elasticity **Eq. 1**, ν is Poisson ratio.

$$E^* = \frac{E}{1-\nu^2}, \quad G^* = \frac{4G}{2-\nu} \tag{3}$$

The forward speed is normalized with respect to the speed of the oscillation and is expressed as the dimensionless variable.

$$\tilde{v}_0 = \frac{v_0}{\omega_{\text{transv}} \cdot u_{\text{lim}}}. \tag{4}$$

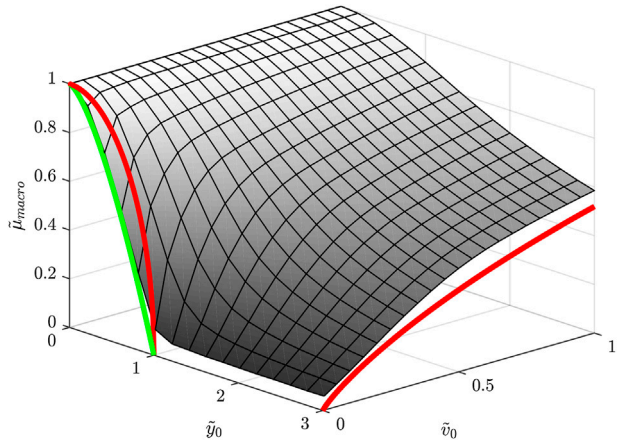

FIGURE 2 | Dependency of the macroscopic coefficient of friction on the dimensionless velocity and oscillation amplitude for transversal oscillations. The smallest value of $\tilde{v}_0$ is 0.005. Green line represents **Eq. (11)**, red lines represent **Eq. (6)** on the right, **Eq. (7)** on the left.

The definitions $\tilde{v}_0$ and $\tilde{y}_0$ coincide with those from Benad et al. (2019) when l_0 of their paper equals u_{lim}, which is the most reasonable interpretation since "l_0 is the elongation at which sliding starts."

The dependent variable is the apparent coefficient of friction $\tilde{\mu}_{\text{macro}}$ which is determined from the tangential force F_x in x-direction and the normal force F_z

$$\tilde{\mu}_{\text{macro}} = \frac{\langle F_x(t)\rangle}{\mu F_z}. \tag{5}$$

Here $\langle\cdots\rangle$ means averaging over one period of oscillation, after the system has tuned in.

Results

Figure 1 shows a typical evolution of the resistive tangential force in x-direction. Such curves were obtained for a variety of combinations for parameters $\tilde{v}_0$ and $\tilde{y}_0$. The resulting macroscopic coefficient of friction is depicted in **Figure 2** and mostly reaffirms known results (Tsai and Tseng, 2005). In Benad et al. (2019), an almost identical graph is not given in the paper but can be found on the cover page of the journal's issue.

Limiting Solution for Large Oscillation Amplitudes

An estimate for the apparent coefficient of friction at large oscillation amplitudes is given as

$$\tilde{\mu}_{\text{macro, large}} = \frac{2}{\pi}\int_0^{\pi/2} \frac{\mathrm{d}\tau}{\sqrt{1+\left(\frac{\tilde{y}_0}{\tilde{v}_0}\sin\tau\right)^2}}. \tag{6}$$

In the range covered in this current work, we find the same as (Benad et al., 2019): We basically confirm **(6)** and find it slightly overestimates the reduction in $\tilde{\mu}_{\text{macro}}$ for finite $\tilde{y}_0$, see the red curve in **Figure 2**. This is to be expected, since the turning points in the oscillation delay the reducing effect.

Limiting Solution for Small Driving Velocities

The limit of small driving velocities can be considered the case of static friction. From a macroscopic point of view, this describes simply the value of the tangential force below which the indenter does not advance. Looking at the situation within an oscillation cycle, the limit translates into the requirement that at least during one infinitesimal instant of the cycle, a forward motion is possible.

In the elastic-single-slider model of (Benad et al., 2019), these instants coincide with the extremal values of the oscillations and a value for the tangential force can be associated. For μ_{macro} a closed form solution at $v_0 \mapsto 0$ is deduced

$$\tilde{\mu}_{\text{macro,static,Benad}} = \sqrt{1-\tilde{y}_0^2} \tag{7}$$

This solution is applicable for $\tilde{y}_0 \le 1$ and is shown in **Figure 2**. For any larger values, static macroscopic friction vanishes.

Our numerical simulations show that **Eq. 7** overestimates the macroscopic friction. In other words, the reduction resulting from the oscillation is underestimated. Here we'd like to argue that this due to the exclusion of partial slip in the model. Partial slip does not occur in a single slider element but requires a finite contact zone and distribution of normal stress.

For a Hertzian indenter in the absence of a forward motion, the oscillation with amplitude $\tilde{y}_0 \le 1$ gives rise to the formation of a ring-shaped slip zone and an inner circle of stick. According to Mindlin theory, the radius of the stick region c depends on $\tilde{y}_0$ according to

$$c = a\sqrt{1-\tilde{y}_0}. \tag{8}$$

where a is the contact radius. From this state, what condition must be met in order to achieve a forward motion? Since $\tilde{v}_0 \mapsto 0$, the oscillations are at high frequency in the outer ring of slip and are very effective in reducing, even suppressing the friction *there*. Therefore it is reasonable to assume that the driving forward motion only has to overcome the friction inside the remaining stick zone. With the total normal force F_z and the normal force only acting inside the stick zone $F_{z,c}$, we can conjecture

$$\tilde{\mu}_{\text{macro,static}} = \frac{F_{z,c}}{F_z} = \frac{\int_0^c p(r)r\mathrm{d}r}{\int_0^a p(r)r\mathrm{d}r}. \tag{9}$$

Here $p(r)$ is the distribution of normal contact stress. In the particular case of a Hertzian stress distribution, **Eq. 9** reduces to

$$\tilde{\mu}_{\text{macro,static}} = 1 - \left(1-\frac{c^2}{a^2}\right)^{3/2} \tag{10}$$

Furthermore in the particular case of translatory oscillations using **Eq. 8** it reduces to

$$\tilde{\mu}_{\text{macro,static}} = 1 - \tilde{y}_0^{3/2} \tag{11}$$

which is also plotted in **Figure 2** and coincides much better with direct simulation results. Thus we see reason that unless the result is zero or one, $\tilde{\mu}_{\text{macro,static}}$ cannot be predicted by a single slider approach.

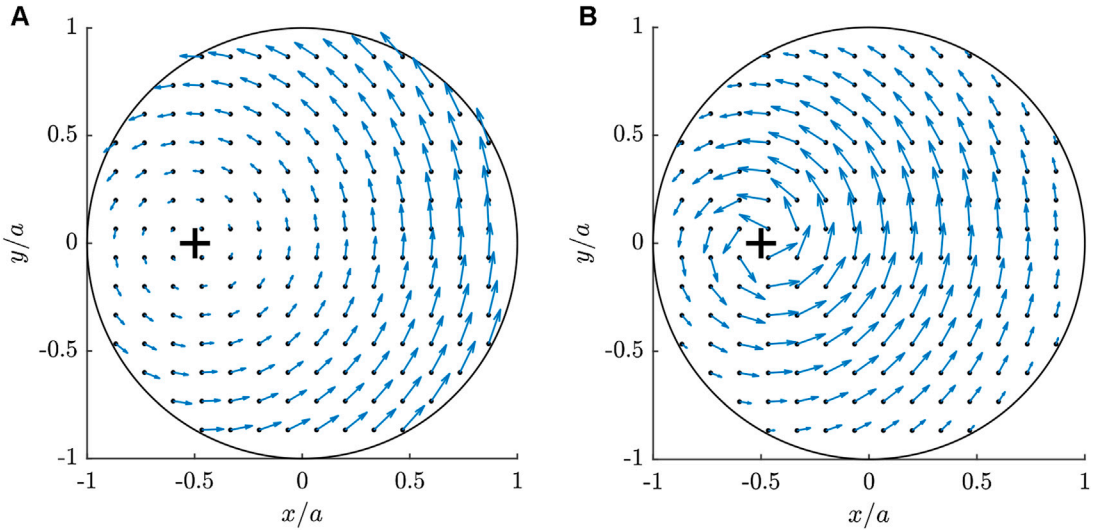

FIGURE 3 | Hertzian indenter slipped in positive *y*-direction and rotated. Normalized forward speed $\tilde{v} = 0.5$. Quiver plots of **(A)** local velocity field, **(B)** tangential surface stresses. The stress vector field also rotates around $x/a = -0.5$ but its amplitude is related to the contact pressure.

CONTINUOUS ROTATION (BORE)

We now investigate a rotationally symmetric indenter which is rotated around the *z*-axis while sliding in the *x*-*y*-plane.

$$\begin{aligned} x(t) &= 0 \\ y(t) &= v_0 t \\ \varphi(t) &= \omega t \end{aligned} \tag{12}$$

Since the problem is quasistatic, it can be reduced to a single system parameter and dimensionless time

$$\tilde{v} = \frac{v_0}{a\omega}, \quad \tilde{t} = \frac{t}{v_0 a} \tag{13}$$

In this configuration, the instantaneous center of rotation in the undeformed remote parts of the body is situated at

$$x_{\text{center}} = -\tilde{v}a, \quad y_{\text{center}} = v_0 t. \tag{14}$$

See **Figure 3A**. The steady state can be analyzed using the following simplifications.

- The velocities of all spots on the surface are assumed to be the same as their corresponding spots in the remote body
- For the calculation of frictional torque, surface stresses are assumed to act at the undeformed spot.

In particular, the above simplifications are valid for small μ. The amplitudes of the frictional stresses τ are given by $|\tau(x,y) = \mu p(x,y)|$ and they are directed opposite to the velocity in each surface point. This can be expressed as

$$\begin{aligned} \tau_x(x,y) &= -\frac{y}{\sqrt{y^2 + (x - x_{\text{center}})^2}} \mu p(x,y) \\ \tau_y(x,y) &= -\frac{(x - x_{\text{center}})}{\sqrt{y^2 + (x - x_{\text{center}})^2}} \mu p(x,y) \end{aligned} \tag{15}$$

See **Figure 3B** for an example. The resulting tangential forces and torque can then be calculated as

$$F_x = 0 \tag{16}$$

$$F_y = \int_o \tau_y \mathrm{d}A = \mu \int_0^a p(r) r Q_Y(r/\tilde{v}a) \mathrm{d}r \tag{17}$$

$$M_z = \int_o \left(\tau_y x - \tau_x y\right) \mathrm{d}A = \mu \int_0^a p(r) r^2 Q_M(r/\tilde{v}a) \mathrm{d}r \tag{18}$$

wherein $\int_0 \mathrm{d}A$ means integrating over the contact area and we introduced

$$Q_Y(\tilde{r}) = \int_0^{2\pi} \frac{\tilde{r}\cos\varphi + 1}{\sqrt{\tilde{r}^2 + 2\tilde{r}\cos\varphi + 1}} \mathrm{d}\varphi \tag{19}$$

$$Q_M(\tilde{r}) = \int_0^{2\pi} \frac{\tilde{r} + \cos\varphi}{\sqrt{\tilde{r}^2 + 2\tilde{r}\cos\varphi + 1}} \mathrm{d}\varphi \tag{20}$$

The additional rotational movement eases the forward movement and effectively reduces the apparent coefficient of friction. Vice versa, the forward motion eases the rotation. Therefore, the required torque M_z also depends on $\tilde{v}$. A macroscopic coefficient of friction can be formulated for both the lateral movement and the rotation.

$$\tilde{\mu}_y(\tilde{v}) = F_y / \mu F_z = \frac{\int_0^1 Q_Y(\tilde{r}/\tilde{v}) p(\tilde{r}a) \tilde{r} \mathrm{d}\tilde{r}}{2\pi \int_0^1 p(\tilde{r}a) \tilde{r} d\tilde{r}} \tag{21}$$

$$\tilde{\mu}_M(\tilde{v}) = M_z / \mu M_{z,0} = \frac{\int_0^1 Q_M(\tilde{r}/\tilde{v}) p(\tilde{r}a) \tilde{r}^2 \mathrm{d}\tilde{r}}{2\pi \int_0^1 p(\tilde{r}a) \tilde{r}^2 \mathrm{d}\tilde{r}} \tag{22}$$

where $M_{z,0}$ is the steady state torque at zero forward velocity.

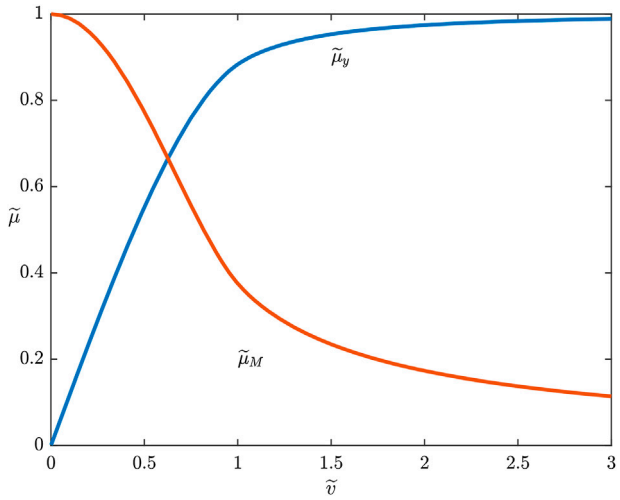

FIGURE 4 | Theoretical prediction of the dependency of the macroscopic coefficient of friction on the dimensionless velocity for added continuous rotational (bore) movement to a Hertzian Indenter according to **Eqs 21** and **22**. The frictional resistances on both the forward motion and on the rotational torque are reduced.

For a Hertzian Indenter the dependencies of **Eqs 21** and **22** on $\tilde{v}$ are shown in **Figure 4**. In our transient numerical simulations, these values are approached after the influence of the initial conditions has vanished. Typical evolutions of the tangential forces and torque are shown in **Figure 5**. It can be seen that the macroscopic forces and torque approach a steady state which is indeed well predicted by **Eqs 21** and **22**.

Interestingly, our simulations never showed zones of stick when the steady state was reached, even when instantaneous center of rotation is located inside the contact region.

OSCILLATING ROTATION (BORE)

In this section, we will set a continuous forward motion and the additional bore rotation will be oscillating. Let us impose a displacement of the indenter according to

$$\begin{aligned} x(t) &= 0 \\ y(t) &= v_0 \cdot t \\ \varphi(t) &= \varphi_0 \sin(\Omega t), \quad \omega = \dot{\varphi} = \varphi_0 \Omega \cos(\Omega t) \end{aligned} \tag{23}$$

Some normalization is again required for the oscillation amplitude. In *"Transverse Oscillations"* section, it was divided by the maximum tangential deflection before the start of macroscopic slip, which is when the inner stick region fully vanishes. In the case of pure rotation of a Hertzian indenter however, there is no such maximum angle at which the stick region vanishes. According to Lubkin (1951) (indexed "lk") (Popov, 2019), the stick radius c and the torsion angle φ are related as

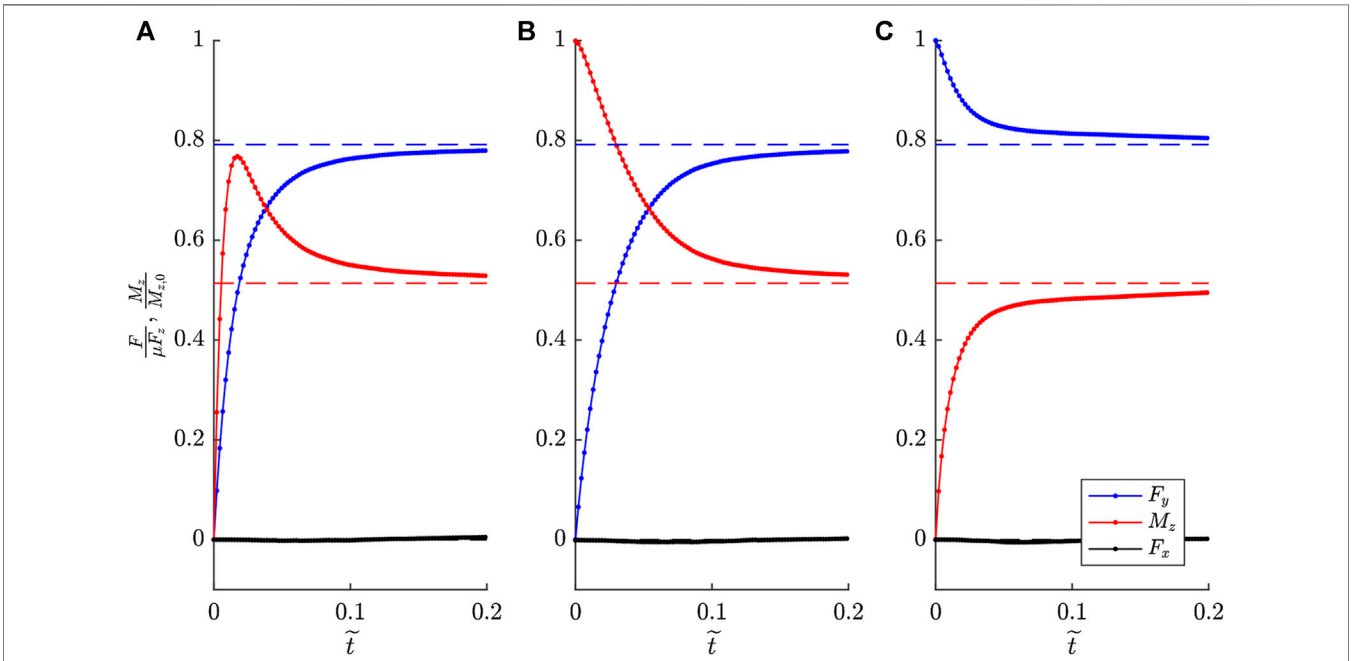

FIGURE 5 | Coefficient of friction regarding Forces and torque of a Hertzian Indenter which is displaced and rotated simultaneously at $\tilde{v} = 0.8$. Dashed lines represent theoretical prediction according to **Eqs 21** and **22**. Initial conditions were **(A)** full stick without tangential stress, **(B)** full rotational slip without lateral displacement and **(C)** full lateral slip, no rotation.

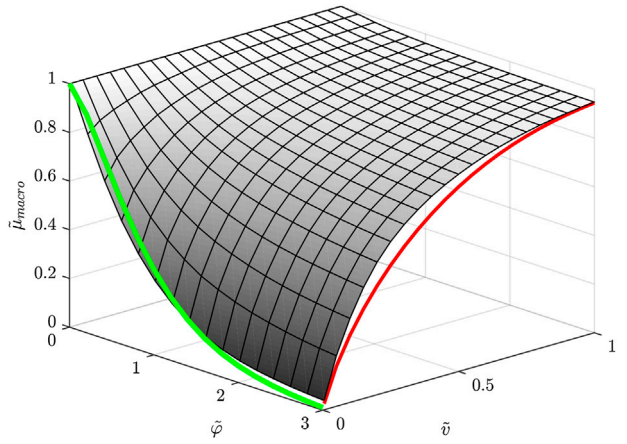

FIGURE 6 | Dependency of the macroscopic coefficient of friction (forward) on the dimensionless velocity and oscillation amplitude for bore oscillations acting on a Hertzian Indenter. The smallest value of $\tilde{v}_0$ is 0.005. Red curve represents the limiting solution according to **Eq. 29** green curve represents **(33)**.

$$\varphi_{lk}(c) = \frac{\mu E^* a}{\pi G R}\left[K\left(\sqrt{1-c^2/a^2}\right) - E\left(\sqrt{1-c^2/a^2}\right)\right] = \frac{u_{\lim}}{a}\frac{4}{\pi(2-\nu)}D(c/a) \tag{24}$$

where we introduced

$$D(m) = K\left(\sqrt{1-m^2}\right) - E\left(\sqrt{1-m^2}\right) \tag{25}$$

With the complete elliptical integrals of the first and second kind

$$K(k) = \int_0^{\pi/2}\left(1-k^2\sin^2\varphi\right)^{-1/2}d\varphi, \qquad E(k) = \int_0^{\pi/2}\left(1-k^2\sin^2\varphi\right)^{1/2}d\varphi \tag{26}$$

Indeed **Eq. 24** tends to infinity for small c, meaning that the very center of the contact will always be in stick state. Normalization of the rotational amplitude will be instead be done with respect to the angle necessary to achieve a stick radius of $c = a/2$ in the absence of lateral displacement.

$$\tilde{\varphi} = \frac{\varphi_0}{\varphi_{lk}(a/2)} = \varphi_0\frac{a}{u_{\lim}}\frac{\pi(2-\nu)}{4D(1/2)} \tag{27}$$

The normalization of the forward velocity is done with respect to the maximum speed of the contact zone edge at $r = a$

$$\tilde{v} = \frac{v_0}{\Omega\varphi_0 a} \tag{28}$$

With these definitions, simulations and evaluation can be done in analogy to *"Transverse Oscillations"* section.

Results

Figure 6 shows the results of μ_{macro} for a range of parameters $\tilde{v}$ and $\tilde{\varphi}$. At first sight, the general appearance resembles the dependencies shown in **Figure 2** of *"Transverse Oscillations"* section. For $\tilde{\varphi} = 0$, no reduction is found and thus $\tilde{\mu}_{macro} = 1$. For large amplitudes of the rotational amplitude, friction is greatly reduced, especially for small forward velocities $\tilde{v}$. Please note however, that even in the limit of $\tilde{v} \mapsto 0$, the macroscopic friction is not reduced to zero.

Limiting Solution for Large Oscillation Amplitudes

For the limiting case of large amplitudes, a similar expression to **Eq. 6** can be found, when it is assumed that the contact is always in a rotational-transversal steady state such as *"Continuous Rotation (Bore)"* section has introduced. Then, the results found in **Eq. 21** can be averaged over one period with momentary values of $\omega(t) = \varphi_0\Omega\cos(\Omega t)$ yielding

$$\tilde{\mu}_{macro,\text{largerot}} = \frac{2}{\pi}\int_0^{\pi/2}\mu_y\left(\frac{v_0}{a\varphi_0\Omega\cos(\tau)}\right)d\tau = \frac{2}{\pi}\int_0^{\pi/2}\mu_y\left(\frac{\tilde{v}}{\cos(\tau)}\right)d\tau \tag{29}$$

This finding is shown in **Figure 6** with the red line. Please note the resemblance to **Eq. 6** in **Figure 2**.

Limiting Solution for Small Driving Velocities

Following the approach laid out in "Limiting Solution for Small Driving Velocities," it is possible to formulate an approximation for the static friction in the limit of $\tilde{v} \mapsto 0$. Let us take the exact same steps for the rotational problem.

In a situation without forward motion, the rotational oscillation will give rise to a zone of constant stick. The oscillation amplitude φ_0 and the static stick radius c are related by **Eq. 24**

$$\varphi_0 = \varphi_{lk}(c) \tag{30}$$

which we can now write in normalized form, introducing $\tilde{c} = c/a$

$$\tilde{\varphi}_{lk}(\tilde{c}) = \frac{\varphi_{lk}(c)}{\varphi_{lk}(a/2)} = \frac{D(\tilde{c})}{D(1/2)} \tag{31}$$

This is a monotonous dependency with $D(1/2) \approx 0.9455$. Let $\tilde{c}_{lk}(\tilde{\varphi})$ be the inverse function

$$\tilde{c}_{lk}(\tilde{\varphi}) = D^{-1}\left[D(1/2)\tilde{\varphi}\right] \tag{32}$$

We can then use this stick radius with **Eq. 10** to find

$$\tilde{\mu}_{macro,static} = 1 - \left(1 - \tilde{c}_{lk}\left(\tilde{\varphi}_0\right)^2\right)^{3/2} \tag{33}$$

Which is shown in **Figure 6** with the green line. It can be seen that **Eq. 33** constitutes a reasonably good prediction of static friction, but not an exact one. It appears to accurately predict the static friction very well for $\tilde{\varphi}_0$ greater than approximately 2. At this point one should note that our judgment on the accuracy is limited, because in order to reach a steady state, the velocities used in the simulation must be strictly positive and smaller values require more computation time. Therefore, the minimum value represented in **Figure 6** is $\tilde{v}_0 = 0.005$. For $\tilde{\varphi}_0 < 2$ however, **Eq. 33** clearly underestimates the reduction of friction.

This means that the forward force does not need to overcome the entire normal stress inside the oscillatory stick zone multiplied with μ, but less. This in turn means that during the forward motion of the indenter, not the entire inner circle slides forward. Indeed, the time series of these simulations indicate that at no point in time there is full sliding in the contact zone. Instead, patches of stick alternate between the left and the right hand side of the contact zone.

CONCLUSIONS

In this paper, we investigate friction under the influence of superposed motion using explicit contact mechanics. In all cases, the superposed motion reduces friction. The stronger the motion (faster, higher amplitude) the greater the reduction. Under the influence of any given superposed motion, the forward friction increases with the forward velocity, stabilizing the frictional system.

Based on the findings presented here for transversal oscillations, the spring model given in Benad et al. (2019) provides satisfactory results, except for very small forward velocities, so-to-speak for static friction when the oscillations provoke some partial slip, which should be taken into account. We postulate that in order to start a forward motion, only the friction inside this stick region must be overcome.

For friction under the influence of additional continuous bore movement, an approximation for the steady state is identified and given in *"Continuous Rotation (Bore)"* section. Both the friction opposing forward motion and opposing the rotation are reduced.

When the bore movement oscillates, a reduction of the macroscopic forward friction is again found and the dependency on forward velocity and oscillation amplitude resembles the transversal case (Compare **Figures 2, 6**). Here, two limiting cases are again identified and analyzed. At large amplitudes, assuming steady state in every instant leads to a good approximation. For small velocities near static friction, a new estimate with good agreement is suggested. It is again based on the stick zone caused by the oscillations alone. However, simulations show that the reduction of forward friction is even greater than predicted, hinting to a more elaborate mechanism.

Rotational bore oscillations are a promising way to control static friction or micro-propulsion due to two favorable properties over transversal oscillations. First, $\tilde{\mu}_{macro,static}$ does not sharply saturate at zero for increasing amplitudes but is instead very well controllable in this region. Second, the reduction in $\tilde{\mu}_{macro,static}$ is very effective even at small amplitudes.

METHOD

We employ the Boundary Elements Method for contact problems (Pohrt and Li, 2014). The normal contact is solved following standard procedures. Interaction of normal and in-plane deformations are not considered. Interactions between the two in-plane directions are considered. For the tangential contact, an iterative scheme is employed that ensures each point satisfies the following conditions in each time step.

- Tangential stress is below the frictional threshold $|\tau| < \mu p$ ("stick state") or,
- Tangential stress $|\tau| = \mu p$ and the difference in point coordinates including deformation, the local velocity, is directed opposite of tangential stress ("slip state")

where τ is the tangential stress, having x and y components, p is the local pressure and μ is the coefficient of friction. For the stress inequality we typically allowed an error of 0.1% and for the alignment of local stresses and velocities we typically allowed an error of 4°. Achieving convergence in the iterative scheme proved be time-consuming. Furthermore, the investigations of low forward speeds required the use of up to 8,000 time steps. As a consequence we limited the spatial resolution of the contact region to 32 times 32 points in bulk simulations such as those shown in **Figures 2, 6**. We used $\nu = 0$ for the Poisson ratio and $\mu = 0.2$.

DATA AVAILABILITY STATEMENT

The raw data supporting the conclusions of this article will be made available by the authors, without undue reservation.

AUTHOR CONTRIBUTIONS

RP developed the BEM code, performed the simulations and created the text and figures.

FUNDING

This research was funded by regular financing of researchers at Technische Universität Berlin.

ACKNOWLEDGMENTS

Discussions with colleagues from TU Berlin were helpful in efforts of the author.

REFERENCES

Ashida, Y., and Aoyama, H. (2007). Press forming using ultrasonic vibration. *J. Mater. Process. Technol.* 187–188, 118–122. doi:10.1016/j.jmatprotec.2006.11.174

Benad, J., Nakano, K., Popov, V. L., and Popov, M. (2019). Active control of friction by transverse oscillations. *Friction* 7 (1), 74–85. doi:10.1007/s40544-018-0202-1

Egashira, K., Mizutani, K., and Nagao, T. (2002).Ultrasonic vibration drilling of microholes in glass. *CIRP Ann.* 51 (1), 339–342. doi:10.1016/S0007-8506(07)61531-5

Fridman, H. D., and Levesque, P. (1959). Reduction of static friction by sonic vibrations. *J. Appl. Phys.* 30 (10), 1572–1575. doi:10.1063/1.1735002

Godfrey, D. (1967). Vibration reduces metal to metal contact and causes an apparent reduction in friction. *Tribol. Trans.* 10, 183–192. doi:10.1080/05698196708972178

Kado, N., Tadokoro, C., and Nakano, K. (2014). Kinetic friction coefficient measured in tribotesting: influence of frictional vibration. *Tribol. Online.* 9 (2), 63–70. doi:10.2474/trol.9.63

Kumar, V. C., and Hutchings, I. M. (2004). Reduction of the sliding friction of metals by the application of longitudinal or transverse ultrasonic vibration. *Tribol. Int.* 37 (10), 833–840. doi:10.1016/j.triboint 2004 05 003

Lenkiewicz, W., (1969). The sliding friction process: effect of external vibrations. *Wear* 13, 99–108. doi:10.1016/0043-1648(69)90505-5

Lubkin, J. L. (1951). The torsion of elastic spheres in contact. *J. Appl. Mech.* 73, 183–187.

Mindlin, R. D. (1949). Compliance of elastic bodies in contact. *J. Appl. Mech.* 16, 259–268.

Murakawa, M. (2001). The utility of radially and ultrasonically vibrated dies in the wire drawing process. *J. Mater. Process. Technol.* 113 (1–3), 81–86. doi:10.1016/S0924-0136(01)00635-5

Pohlman, R., and Lehfeldt, E. (1966). Influence of ultrasonic vibration on metallic friction. *Ultrasonics* 4 (4), 178–185. doi:10.1016/0041-624X(66)90244-7

Pohrt, R., and Li, Q. (2014). Complete boundary element formulation for normal and tangential contact problems. *Phys. Mesomech.* 17 (4), 334–340. doi:10.1134/S1029959914040109

Popov, M., and Li, Q. (2018). Multimode active control of friction, dynamic ratchets and actuators. *Phys. Mesomech.* 21 (1), 24–31. doi:10.1134/s1029959918010046

Popov, V. L., Heß, M., and Willert, E. (2019). *Handbook of contact mechanics. Exact solutions of axisymmetric contact problems.* 1st Edn. Berlin: Springer-Verlag, 347.

Siegert, K., and Ulmer, J. (2001a). Influencing the friction in metal forming process by superimposing ultrasonic waves. *CIRP Ann.* 50 (1), 195–200. doi:10.1016/S0007-8506(07)62103-9

Siegert, K., and Ulmer, J. (2001b). Superimposing ultrasonic waves on the dies in tube and wire drawing. *J. Eng. Mater. Technol.* 123 (4), 517–523. doi:10.1115/1.1397779

Starcevic, J., and Filippov, A. E. (2012). Simulation of the influence of ultrasonic in-plane oscillations on dry friction accounting for stick and creep. *Phys. Mesomech. Mesomech.* 15 (5–6), 330–332. doi:10.1134/S1029959912030150

Storck, H. (2002). The effect of friction reduction in presence of ultrasonic vibrations and its relevance to travelling wave ultrasonic motors. *Ultrasonics* 40, 1–8. doi:10.1016/s0041-624x(02)00126-9

Teidelt, E. (2012). Influence of ultrasonic oscillation on static and sliding friction, *Tribol. Lett.* 48, 51–62. doi:10.1007/s11249-012-9937-4

Teidelt, E., Willert, E., Filippov, A. E., and Popov, V. L. (2012). Modeling of the dynamic contact in stick-slip microdrives using the method of reduction of dimensionality. *Phys. Mesomech.* 15 (5–6), 287–292. doi:10.1134/S1029959912030071

Thomsen, J. (1999). Using fast vibrations to quench friction-induces oscillations. *J. Sound Vib.* 228, 1079–1102. doi:10.1006/jsvi.1999.2460

Tsai, C. C., and Tseng, C. H. (2005). The effect of friction reduction in the presence of in-plane vibrations. *Arch. Appl. Mech.* 75, 164–176. doi:10.1007/s00419-005-0427-0

Conflict of Interest: The author declares that the research was conducted in the absence of any commercial or financial relationships that could be construed as a potential conflict of interest.